



## FULL PAPER

# Synthesis, characterization and $\alpha$ -amylase and $\alpha$ -glucosidase inhibition studies of novel vanadyl chalcone complexes

Mandeep Kaur | Raj Kaushal

Department of Chemistry, National Institute of Technology, Hamirpur, India

**Correspondence**

Raj Kaushal, Department of Chemistry, National Institute of Technology, Hamirpur, 177005 Himachal Pradesh, India.

Email: rajkaushal@nith.ac.in

A series of chalcone ligands and their corresponding vanadyl complexes of composition  $[\text{VO}(\text{L}^{\text{I-IV}})_2(\text{H}_2\text{O})_2]\text{SO}_4$  (where  $\text{L}^{\text{I}} = 1,3\text{-Diphenylprop-2-en-1-one}$ ,  $\text{L}^{\text{II}} = 3\text{-}(2\text{-Hydroxy-phenyl})\text{-1-phenyl-propenone}$ ,  $\text{L}^{\text{III}} = 3\text{-}(3\text{-Nitro-phenyl})\text{-1-phenyl-propenone}$ ,  $\text{L}^{\text{IV}} = 3\text{-}(4\text{-Methoxy-phenyl})\text{-1-phenyl-propenone}$ ) have been synthesized and characterized using various spectroscopic (Fourier-transform infrared, electrospray ionization mass, nuclear magnetic resonance, electron paramagnetic resonance, thermogravimetric analysis, vibrating sample magnetometer) and physico-analytic techniques. Antidiabetic activities of synthesized complexes along with chalcones were evaluated by performing *in vitro* and *in silico*  $\alpha$ -amylase and  $\alpha$ -glucosidase inhibition studies. The obtained results displayed moderate to significant inhibition activity against both the enzymes by vanadyl chalcone complexes. The most potent complexes were further investigated for the enzyme kinetic studies and displayed the mixed inhibition for both the enzymes. Further, antioxidant activity of vanadyl chalcone complexes was evaluated for their efficiency to release oxidative stress using 2,2-diphenyl-1-picryl-hydrazyl-hydrate assay, and two complexes (Complexes **2** and **4**) have demonstrated remarkable antioxidant activity. All the complexes were found to possess promising antidiabetic and antioxidant potential.

**KEYWORDS**docking, enzyme inhibition, vanadyl chalcone complexes,  $\alpha$ -amylase,  $\alpha$ -glucosidase

## 1 | INTRODUCTION

Vanadium is a critically important element from biological point of view,<sup>[1]</sup> especially coordination chemistry of Oxidation States III, IV and V that show pronounced significance in water.<sup>[2]</sup> Therapeutic potency of its complexes is obvious from its application in nitrogen fixation,<sup>[3]</sup> used as halo-peroxidases,<sup>[4]</sup> antitumour activity,<sup>[5]</sup> insulin-mimetic action,<sup>[6]</sup> cleavage and binding of DNA<sup>[7]</sup> and antioxidant properties.<sup>[8]</sup> This pivotal role of vanadium in biological and chemical processes

encouraged the progress of vanadium chemistry. As  $\text{VO}^{2+}$  is less toxic than other oxidation states due to its stable bio-state condition in organs,<sup>[9]</sup> it is being monitored for its hypoglycemic effect since the 19th century because of its insulin-mimetic action.<sup>[10]</sup> The highly conjugated chalcone and its derivatives as ligands have captivated scientists' attention due to its reactive carbonyl group,<sup>[11]</sup> varied range of biological activities, diversity of substituents and ease of synthesis.<sup>[12]</sup> Therefore, chalcones and its metal complexes have induced broad spectrum of biological potential and have been used in traditional medicine for so long.<sup>[13]</sup> The antidiabetic activity of the chalcones was most prominent

**Abbreviations:** DPPH, 2,2-diphenyl-1-picryl-hydrazyl-hydrate..

from the extensive range of activities, and many key structural features are already acknowledged in the literature.<sup>[14]</sup> Diabetes mellitus (DM) is a prevalent global burden of disease now. It is the third leading cause of mortality worldwide.<sup>[15]</sup> According to the World Health Organization report, more than 400 million people live with diabetes worldwide. In 2016, it was the seventh leading cause of death. Almost 90% cases of diabetes out of total are of type 2 DM.<sup>[16]</sup> Chronic diabetes is associated with many postprandial effects like premature dying, blindness, obesity, cataracts, kidney failure, heart attack, fatty liver disease, stroke and lower limb amputation.<sup>[17]</sup> During the ongoing Covid-19 pandemic, it was observed that the chances of diabetic patients to get infected with the virus are 5%–18% more than the others. Moreover, during the SARS-CoV-1 outbreak in 2002–2003, diabetes was the sole independent factor to increase the complications.<sup>[18]</sup> Since the last few decades, diabetes status has increased from mild disorder to one of the foremost reason for morbidity and mortality among the population.<sup>[19]</sup> Now, chalcones and its metal complexes exert hypoglycemic properties by targeting the different enzymes involved in the metabolic and digestion processes such as tyrosine phosphatase,  $\alpha$ -glucosidase  $\alpha$  amylase, aldose reductase and dipeptidyl peptidase 4.<sup>[20]</sup> Actually, by retardation of the hyperactivity of the  $\alpha$ -cells (amylase and glucosidase), blood glucose level is lowered.<sup>[21]</sup> Inhibition of these enzymes delays the digestion of carbohydrate and slows down the glucose absorption rate, which depresses the postprandial hyperglycemia.<sup>[22]</sup> For example, acarbose, miglitol and voglibose are few drugs already used in clinical practice. Still, the currently available anti-diabetic drugs do not present the desired efficacy and are generally associated with serious adverse side effects.<sup>[14]</sup>

As stated above, vanadium complexes and chalcones both induces great therapeutic potential, but an area of complexation of vanadium metal with chalcones has been less explored. In 2017, Atlam et al.<sup>[23]</sup> synthesized the vanadium complex with DMATP chalcone, and complex was found to possess great deal of DNA binding and antimicrobial potential but did not study its antidiabetic potential. So, in this present study, four vanadium chalcone complexes were synthesized and characterized using Fourier-transform infrared (FTIR), electrospray ionization (ESI) mass, nuclear magnetic resonance (NMR), electron paramagnetic resonance (EPR) and thermogravimetric analysis (TGA) studies. Additionally, their antioxidant activity is analysed on 2,2-diphenyl-1-picryl-hydrazyl-hydrate (DPPH), and antidiabetic potential is monitored against  $\alpha$ -glucosidase and  $\alpha$ -amylase enzymes.

## 2 | EXPERIMENTAL

### 2.1 | Materials and chemicals

Analytical reagent (AR)-grade chemicals and solvents were employed as received for the synthesis of organic ligands. Acetophenone, benzaldehyde, 2-hydroxybenzaldehyde, 3-Nitrobenzaldehyde, 4-Anisaldehyde, ethanol, sodium hydroxide, hydrochloric acid, dimethylsulphoxide, phosphate buffer, DPPH, *p*-nitrophenyl- $\alpha$ -D-glucopyranoside, *Aspergillus oryzae*  $\alpha$ -amylase, Acarbose and  $\alpha$ -glucosidase were purchased from Sigma Aldrich and Himedia.

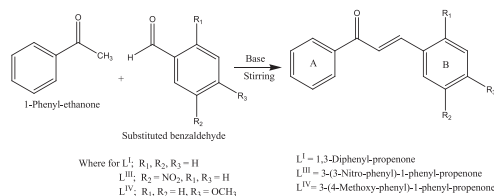
### 2.2 | Physical measurements

Determination of the melting point was carried out on paramount digital melting point apparatus. Infrared stretching frequencies were recorded in the range 400–4,000  $\text{cm}^{-1}$ . Electron paramagnetic spectroscopy study was performed on ESR-JEOL (JES-FA200 ESR Spectrometer with X and Q band). ESI mass spectrum was performed with XEVO G2-XS QTOF. <sup>1</sup>H-NMR spectrum was recorded on JEOL PECX 500 MHz spectrometer. TGA thermogram was recorded using SDT Q600 V20.9 Build 20 facility. The molar conductivity was measured with the alpha-06 digital conductivity metre. The biological activities were analysed using microprocessor ultraviolet-visible (UV-Vis) spectrophotometer (double beam LI-2800). Surface morphology was monitored by scanning electron microscope (SEM).

### 2.3 | Synthesis of chalcone ligands

Chalcones were synthesized by the classical Claisen-Schmidt method.<sup>[24]</sup> All the ligands were prepared either by stirring or by a solvent-free grinding method as described as follows:

Method A: 1,3-Diphenylprop-2-en-1-one, 3-(3-Nitro-phenyl)-1-phenyl-propenone and 3-(4-Methoxy-phenyl)-1-phenyl-propenone ligands were synthesized by stirring ethanolic solution of acetophenone (100 mg, 8.3 mmol) and substituted benzaldehyde in 1:1 molar ratio. NaOH solution was added gradually till the yellow-coloured precipitates were formed. After 5 h of stirring, the mixture was neutralized with 0.2 N HCl solutions to eliminate the excess base. Yellow-coloured precipitates were vacuum-filtered, washed with ethanol and dried in the open. General scheme for the synthesis of Chalcones  $L^{I-III}$  is shown in Scheme 1.



**SCHEME 1** General reaction scheme for the synthesis of Chalcones L<sup>I</sup>, L<sup>III-IV</sup>

### 2.3.1 | 1,3-Diphenylprop-2-en-1-one (L<sup>I</sup>)

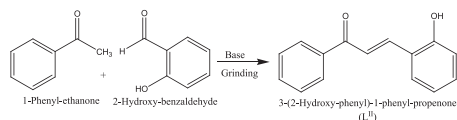
Yield: 74.56, m.p.: 57°C; FTIR spectrum (KBr;  $\bar{\nu}$  cm<sup>-1</sup>): 3062 (=CH), 1,662 (C=O); <sup>1</sup>H NMR (H<sub>2</sub>O-d<sub>2</sub>, 500 MHz)  $\delta$  (ppm): 7.83 (d, 1H, J = 15.8 Hz; H<sub>A</sub>), 7.52 (d, 1H, J = 15.8 Hz; H<sub>B</sub>), Ring A, 8.03 (t, 2H), 7.65 (m, 2H), 7.58 (t, 1H), Ring B, 7.50 (t, 2H), 7.42 (m, 3H); <sup>13</sup>C NMR (H<sub>2</sub>O-d<sub>2</sub>, 500 MHz)  $\delta$  (ppm): 190.5 (C=O), 144.7 (C<sub>A</sub>), 122.7 (C<sub>B</sub>); ESI mass (*m/z* %): 209.10 (MH<sup>+</sup>, 100), 191.09, 152.07.

### 2.3.2 | 3-(3-Nitro-phenyl)-1-phenyl-propenone (L<sup>III</sup>)

Yield: 80.69, m.p.: 155°C; FTIR spectrum (KBr;  $\bar{\nu}$  cm<sup>-1</sup>): 3,073 (=CH), 1,605 (C=O), 1,568 (NO<sub>2</sub> $\nu_{as}$ ), 1,366 (NO<sub>2</sub> $\nu_s$ ); <sup>1</sup>H NMR (H<sub>2</sub>O-d<sub>2</sub>, 500 MHz)  $\delta$  (ppm): 7.9 (d, 1H, J = 8.25 Hz; H<sub>A</sub>), 7.86 (d, 1H, J = 15.8 Hz; H<sub>B</sub>), Ring A, 8.11 (d, 2H), 7.56 (t, 2H), Ring B, 8.52 (s, 1H), 8.28 (d, 1H); <sup>13</sup>C NMR (H<sub>2</sub>O-d<sub>2</sub>, 500 MHz)  $\delta$  (ppm): 189.6 (C=O), 141.6 (C<sub>A</sub>), 122.3 (C<sub>B</sub>); ESI mass (*m/z* %): 254 (MH<sup>+</sup>, 100), 230, 209, 176.

### 2.3.3 | 3-(4-Methoxy-phenyl)-1-phenyl-propenone (L<sup>IV</sup>)

Yield: 72.34, m.p.: 92°C; FTIR spectrum (KBr;  $\bar{\nu}$  cm<sup>-1</sup>): 3,063 (=CH), 2,954 (—CH), 1,660 (C=O), 1,163 (C—O—C); <sup>1</sup>H NMR (H<sub>2</sub>O-d<sub>2</sub>, 500 MHz)  $\delta$  (ppm): 7.08 (d, 1H, J = 15.8 Hz; H<sub>A</sub>), 7.43 (d, 1H, J = 15.1 Hz; H<sub>B</sub>), Ring A- 8.02 (t, 2H), 7.62 (m, 3H), Ring B- 7.51 (t, 2H), 6.95 (t, 2H), 3.86 (s, 3H); <sup>13</sup>C NMR (H<sub>2</sub>O-d<sub>2</sub>, 500 MHz)  $\delta$  (ppm): 190.5 (C=O), 144.7 (C<sub>A</sub>), 119.7 (C<sub>B</sub>), 55.3 (—OCH<sub>3</sub>); ESI mass (*m/z* %): 239 (MH<sup>+</sup>, 100), 237, 189.



**SCHEME 2** Reaction scheme for the synthesis of 3-(2-Hydroxy-phenyl)-1-phenyl-propenone (L<sup>II</sup>)

Method B: synthesis of 3-(2-Hydroxy-phenyl)-1-phenyl-propenone was carried out by grinding 1-Phenylethanone and 2-Hydroxy benzaldehyde in 1:1 molar ratio using mortar and pestle with NaOH for 10–15 min till the mass thickens. Then, the solidified mass was dissolved in water and neutralized with 0.2 M HCl, and precipitates of chalcone (L<sup>IV</sup>) were vacuum-filtered, washed with ethanol and dried in air.<sup>[25]</sup> The reaction scheme is shown in Scheme 2.

### 2.3.4 | 3-(2-Hydroxy-phenyl)-1-phenyl-propenone (L<sup>II</sup>)

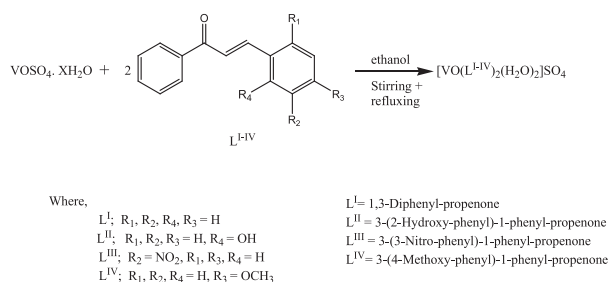
Yield: 86.72, m.p.: 125°C; FTIR spectrum (KBr;  $\bar{\nu}$  cm<sup>-1</sup>): 3,565 (—OH), 3,053 (=CH), 1,668 (C=O); <sup>1</sup>H NMR (H<sub>2</sub>O-d<sub>2</sub>, 500 MHz)  $\delta$  (ppm): 10.03 (1H, s, OH, D<sub>2</sub>O exchangeable), 8.22 (d, 1H, J = 15.8 Hz; H<sub>A</sub>), 7.97 (d, 1H, J = 6.9 Hz; H<sub>B</sub>), 7.64–7.20 (m, 5Hs of Ring A), 6.67–6.51 (m, 4Hs of Ring B); <sup>13</sup>C NMR (H<sub>2</sub>O-d<sub>2</sub>, 500 MHz)  $\delta$  (ppm): 194 (C=O), 174 (C—OH), 146 (C<sub>A</sub>), 123 (C<sub>B</sub>); ESI mass (*m/z* %): 225.10 (MH<sup>+</sup>), 207, 183, 165.

## 2.4 | Synthesis of vanadyl chalcone complexes [VO (L<sup>I-IV</sup>)<sub>2</sub>(H<sub>2</sub>O)<sub>2</sub>]<sub>2</sub>SO<sub>4</sub> (1–4)

Vanadyl chalcone complexes were prepared according to method reported by Atlam et al.<sup>[23]</sup> with certain modifications. The ethanolic solution of VOSO<sub>4</sub>·xH<sub>2</sub>O (0.0012 moles) was mixed with the ethanolic solution of L<sup>I-IV</sup> (0.0024 moles) in a 1:2 molar ratios with continuous stirring followed by dropwise addition of 20 ml of 0.1 M solution of NaOH. Then, the reaction mixture was refluxed for about 10 h. During the course of reaction, a green-coloured precipitate of the complex was separated out. The precipitates of the desired complex were filtered under vacuum and washed with ethanol for three–four times. The reaction can be rationalized in the form of chemical equation as represented in Scheme 3.

### 2.4.1 | [VO (L<sup>I</sup>)<sub>2</sub> (H<sub>2</sub>O)<sub>2</sub>]<sub>2</sub>SO<sub>4</sub> (1)

Yield (%): 69.33, m.p.: >300°C; paramagnetic; FTIR spectrum (KBr;  $\bar{\nu}$  cm<sup>-1</sup>): 3,483 (OH), 1,615 (C=O), 1,119, 616 (SO<sub>4</sub>), 966 (V=O), 513 (V—O), 674 (Coord. H<sub>2</sub>O). ESI mass (*m/z* %): 615 (molar mass), 541 ([VO (L<sup>I</sup>)<sub>2</sub>(H<sub>2</sub>O)<sub>2</sub>]<sub>2</sub>Na<sup>+</sup>, 453 ([VO(L<sup>I</sup>)(C<sub>7</sub>H<sub>5</sub>O)(H<sub>2</sub>O)<sub>2</sub>]<sub>2</sub>K<sup>+</sup>, 274 (VO(L<sup>I</sup>), 230 (L<sup>I</sup>)Na, 209 (L<sup>I</sup>H<sup>+</sup>);  $\Lambda_M = 54.15 \Omega^{-1} \text{ cm}^2 \text{ mol}^{-1}$  in mM solution of DMSO;  $g_{iso} = 1.9978$ .



**SCHEME 3** General reaction scheme for the synthesis of  $[\text{VO}(\text{L}^{\text{I-IV}})_2(\text{H}_2\text{O})_2]\text{SO}_4$  complexes (**1-4**)

### 2.4.2 | $[\text{VO}(\text{L}^{\text{II}})_2(\text{H}_2\text{O})_2]\text{SO}_4$ (2)

Yield (%): 76.30, m.p.:  $>300^\circ\text{C}$ ; paramagnetic; FTIR spectrum (KBr;  $\bar{\nu}\text{cm}^{-1}$ ): 3,447 (OH), 1,589 (C=O), 1,120, 619 ( $\text{SO}_4$ ), 970 (V=O), 519 (V—O), 705 (Coord.  $\text{H}_2\text{O}$ ). ESI mass ( $m/z$  %): 646 (molar mass), 480 ( $[\text{VO}(\text{L}^{\text{II}})(\text{H}_2\text{O})_2(\text{C}_9\text{H}_7\text{O})]\text{Na}^+$ , 470 ( $[\text{VO}(\text{L}^{\text{II}})(\text{H}_2\text{O})_2(\text{C}_7\text{H}_5\text{O})]\text{K}^+$ , 430 ( $[\text{VO}(\text{L}^{\text{II}})(\text{H}_2\text{O})_2(\text{C}_7\text{H}_5\text{O})]\text{H}^+$ , 308 ( $[\text{VO}(\text{L}^{\text{II}})(\text{H}_2\text{O})_2]\text{Na}^+$ , 263 ( $[\text{L}^{\text{II}}]\text{K}^+$ , 207 ( $[\text{L}^{\text{II}}-\text{OH}]$ );  $\Lambda_{\text{M}} = 89.32 \Omega^{-1} \text{cm}^2 \text{mol}^{-1}$  in mM solution of DMSO;  $g_{\text{iso}} = 1.9869$ .

### 2.4.3 | $[\text{VO}(\text{L}^{\text{III}})_2(\text{H}_2\text{O})_2]\text{SO}_4$ (3)

Yield (%): 62.59, m.p.:  $>300^\circ\text{C}$ ; paramagnetic; FTIR spectrum (KBr;  $\bar{\nu}\text{cm}^{-1}$ ): 3432 (OH), 1,598 (C=O), 1,113, 621 ( $\text{SO}_4$ ), 957 (V=O), 528 (V—O), 775 (Coord.  $\text{H}_2\text{O}$ ). ESI mass ( $m/z$  %): 679 for  $[\text{VO}(\text{L}^{\text{III}})_2(\text{H}_2\text{O})_2]\text{SO}_4 + \text{Na}$ , 342 for  $(\text{VOL}^{\text{III}})\text{Na}^+$ , 276 for  $(\text{L}^{\text{III}}) + \text{Na}^+$ ;  $\Lambda_{\text{M}} = 50.32 \Omega^{-1} \text{cm}^2 \text{mol}^{-1}$  in mM solution of DMSO;  $g_{\text{iso}} = 1.9856$ .

### 2.4.4 | $[\text{VO}(\text{L}^{\text{IV}})_2(\text{H}_2\text{O})_2]\text{SO}_4$ (4)

Yield (%): 48.21, m.p.:  $>300^\circ\text{C}$ ; paramagnetic; FTIR spectrum (KBr;  $\bar{\nu}\text{cm}^{-1}$ ): 3,465 (OH), 1,639 (C=O), 1,115, 612 ( $\text{SO}_4$ ), 965 (V=O), 528 (V—O), 783 (Coord.  $\text{H}_2\text{O}$ ). ESI mass ( $m/z$  %): 239 (for  $\text{L}^{\text{IV}} + \text{H}^+$ ), 274 (for  $\text{L}^{\text{IV}} - 3\text{H} + \text{K}^+$ , 340 [for  $\text{VO}(\text{L}^{\text{IV}})(\text{H}_2\text{O})_2$ ], 540 (for  $[\text{VO}(\text{L}^{\text{IV}})(\text{H}_2\text{O})_2(\text{C}_{10}\text{H}_9\text{O}_2)]\text{K}^+$ ,  $\Lambda_{\text{M}} = 53.29 \Omega^{-1} \text{cm}^2 \text{mol}^{-1}$  in mM solution of DMSO;  $g_{\text{iso}} = 1.9993$ .

## 2.5 | Antioxidant activity

Synthesized chalcones ligands ( $\text{L}^{\text{I-IV}}$ ) and their respective vanadyl complexes of chemical composition  $[\text{VO}(\text{L}^{\text{I-IV}})_2(\text{H}_2\text{O})_2]\text{SO}_4$  (**1-4**) were evaluated for their antioxidant activity using the DPPH radical scavenging

assay method with some changes.<sup>[26]</sup> In brief, fixed volume of 0.1 mM solution of DPPH in ethanol was added to different concentrations (5, 20, 50, 80, 100, 150, and 300  $\mu\text{M}$ ) of the prepared ligand and vanadyl chalcone complexes (**1-4**) in dark. Then, the solution was incubated for 1 h at room temperature for reaction completion. Absorbance was recorded for each dilution at 517 nm against reference control (ascorbic acid) at the same wavelength. A graph was plotted between concentration (on the abscissa) and % inhibition (on the ordinate) to calculate  $\text{IC}_{50}$  value. The % inhibition for DPPH radical was evaluated according to the following equation:

$$\text{DPPH radical scavenging activity or (\% inhibition)} = \frac{A_0 - A_1}{A_0} \times 100, \quad (1)$$

where  $A_0$  = absorbance of control reaction and  $A_1$  = absorbance in presence of test sample.

## 2.6 | Antidiabetic activity

### 2.6.1 | Alpha-glucosidase inhibition assay

The synthesized complexes were evaluated for  $\alpha$ -glucosidase inhibitory activity against  $\alpha$ -glucosidase extracted from yeast. The investigation was carried out according to a previously reported *p*NPG method incorporating few modifications.<sup>[27]</sup> In short, 10  $\mu\text{L}$  of  $\alpha$ -glucosidase enzyme solution of 5 U/ml prepared in ice-cold phosphate buffer (pH 6.9) was added to different concentrations (3, 6, 10, 15, 20, and 50  $\mu\text{M}$ ) of the ligands and their vanadyl chalcone complexes and incubated for 20 min at  $37^\circ\text{C}$ . After incubation, the addition of 200  $\mu\text{L}$  of 1 mM *p*NPG solution was carried out to the solution followed by the incubation for 30 min at  $37^\circ\text{C}$ . The reaction was ceased off by pouring 200  $\mu\text{L}$  of  $\text{Na}_2\text{CO}_3$  into the reaction vessel. UV-Vis spectrophotometer used to record the absorbance of yellow colour solution due to the liberation of *p*-nitrophenol at wavelength 405 nm and % inhibition was calculated using Equation 2.  $\text{IC}_{50}$  values were computed from the plot of concentration *v/s* % inhibition. Acarbose was taken as the standard reference.

$$\text{Inhibition activity (\%)} = \left( \frac{A_b - A_s}{A_b} \right) \times 100, \quad (2)$$

where  $A_s$  and  $A_b$  correspond to the absorbance of the sample under investigation, blank (with no sample), respectively.

## 2.6.2 | Alpha-amylase inhibition assay

$\alpha$ -amylase inhibition assay was performed in vitro by using iodine starch method as described in the study of Zhang and Kim amending slightly.<sup>[28]</sup> To prepare the reaction mixture, 10  $\mu$ l of 20 u/ml of  $\alpha$ -amylase (extracted from *A. oryzae*) was dissolved in 10 mM phosphate buffer (pH 6.9, NaCl 6 mM) and mixed with varying concentrations of the test sample. The reaction mixture was then incubated for 30 min at 37°C. After incubation, 100  $\mu$ l of 1% starch solution was poured into it and incubated for 20 min at 37°C. The reaction was terminated by adding 100  $\mu$ l of 1 M HCl to the reaction mixture, and 200  $\mu$ l of iodine solution was added afterwards. The quantification of the colour imparted to the reaction mixture by iodine solution (as yellow colour of iodine changes to deep blue colour if starch is present) was done spectrometrically at 620 nm wavelength. Percentage inhibition of activity was calculated from the following equation:

$$\% \text{inhibition activity} = \left[ \frac{A_s - A_b}{A_c - A_b} \right] \times 100, \quad (3)$$

where  $A_s$  = absorbance of the test sample,  $A_b$  = absorbance of the blank (excluding starch and test sample) and  $A_c$  = absorbance of the control (excluding  $\alpha$ -amylase and test sample).

A graph was plotted between the concentration of the test sample and its inhibitory activity (%) to determine the  $IC_{50}$  value and compared with the standard reference acarbose (commercially used  $\alpha$ -amylase inhibitor).

## 2.6.3 | Enzyme kinetics and mode of inhibition

Kinetics studies for  $\alpha$ -glucosidase and  $\alpha$ -amylase were performed in order to determine the mode of inhibition followed by vanadyl complex inhibitors. Different concentrations of substrate (*p*-nitrophenyl- $\alpha$ -D-glucopyranoside for  $\alpha$ -glucosidase and starch for  $\alpha$ -amylase) were used in the presence of different concentrations of the test sample with the best  $IC_{50}$  value. A test sample of control (0  $\mu$ M), 10  $\mu$ M concentration was used for  $\alpha$ -glucosidase and for  $\alpha$ -amylase. Michaelis–Menten equation (Equation 4) and Lineweaver–Burk double-reciprocal plot ( $1/V$  vs  $1/[S]$ ) was employed to discern the  $V_{max}$ ,  $K_{max}$  and mode of inhibition.<sup>[29]</sup>

$$\frac{1}{V} = \frac{K_m}{V_{max}[S]} + \frac{1}{V_{max}}, \quad (4)$$

where  $V_{max}$  is the maximal velocity,  $[S]$  is the substrate concentration and  $K_m$  is the Michalis constant.

## 2.7 | In silico $\alpha$ -amylase and $\alpha$ -glucosidase inhibition studies of vanadyl chalcone complexes

The binding modes of  $\alpha$ -amylase and  $\alpha$ -glucosidase enzyme with synthesized complexes (**1–4**) were investigated with the help of molecular docking using autodock tool 1.5.6. The 3D structure of the chalcones and their vanadyl complexes were obtained from ACD/chemsketch in MDL molfiles (V2000) format. The 3vx0.pdb and 3w37.pdb files were downloaded from Protein data bank for the structure of  $\alpha$ -amylase and  $\alpha$ -glucosidase, respectively. These files were processed for energy minimization using Swiss-Pdb viewer 4.1.0. and got it ready for docking. The autodock input files were created using autodock tool 1.5.6 software. The docked files were processed using cygwin64 software, and UCSF Chimera software was employed to visualize the docked poses.

## 3 | RESULTS AND DISCUSSION

### 3.1 | Synthesis, characterization of chalcone and their vanadium complexes

The synthesis of vanadium chalcone complexes was carried out as the scheme presented in Scheme 3. Complexes were dark green-coloured fine powder of amorphous nature and are stable at standard temperature and pressure. The related analytical and physical data are summarized in Table 1 and discussed in the following sections.

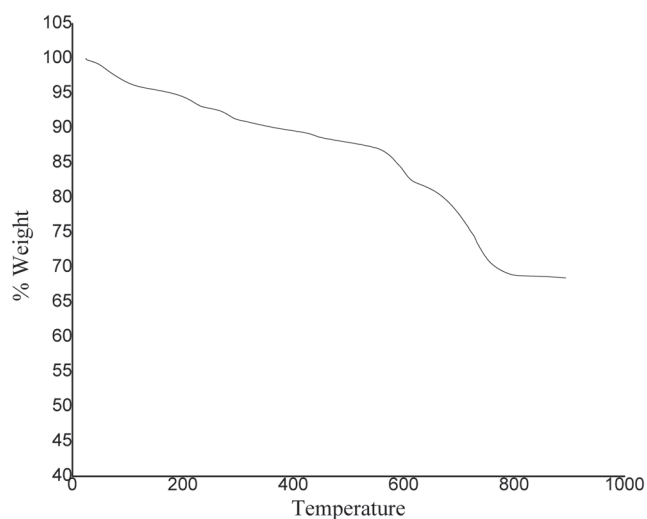
#### 3.1.1 | FTIR spectral data

The resultant FTIR spectral data of complexes (Figures S5–S8) are reported after comparing with their respective ligands (Figures S1–S4). FTIR spectra of synthesized vanadyl chalcone complexes show the appearance of the strong but broad absorption band in the range of 3,483–3,432  $cm^{-1}$  due to  $\nu_{OH}$  stretching vibration of the  $H_2O$  molecule in the complexes.<sup>[30]</sup> Bonding mode of the water molecule was further verified by the presence of an absorption band in range 650–800  $cm^{-1}$ , which appears due to the coordinated mode of a water molecule.<sup>[31]</sup> TGA analysis was further carried out to establish the presence of water molecule in coordination sphere. From the graph in Figure 1, 4.9% weight loss was observed at 142°C temperature, which was assigned to

**TABLE 1** Important infrared-spectrum bands ( $\bar{\nu}$  cm<sup>-1</sup>) of chalcones (L<sup>I-IV</sup>) and [VO (L<sup>I-IV</sup>)<sub>2</sub>(H<sub>2</sub>O)<sub>2</sub>]<sub>2</sub>SO<sub>4</sub> (1–4) complexes

Ligand/complexes	OH	—C=O	V=O	V—O	Coordinated H <sub>2</sub> O	SO <sub>4</sub> ion
L <sup>I</sup>	-	1,662	-	-	-	-
L <sup>II</sup>	3,665	1,668	-	-	-	-
L <sup>III</sup>	-	1,605	-	-	-	-
L <sup>IV</sup>	-	1,660	-	-	-	-
[VO (L <sup>I</sup> ) <sub>2</sub> (H <sub>2</sub> O) <sub>2</sub> ] <sub>2</sub> SO <sub>4</sub> (1)	3,483	1,615	966	513	674	1,119, 616
[VO (L <sup>II</sup> ) <sub>2</sub> (H <sub>2</sub> O) <sub>2</sub> ] <sub>2</sub> SO <sub>4</sub> (2)	3,447	1,589	970	519	705	1,120, 619
[VO (L <sup>III</sup> ) <sub>2</sub> (H <sub>2</sub> O) <sub>2</sub> ] <sub>2</sub> SO <sub>4</sub> (3)	3,432	1,598	957	528	775	1,113, 621
[VO (L <sup>IV</sup> ) <sub>2</sub> (H <sub>2</sub> O) <sub>2</sub> ] <sub>2</sub> SO <sub>4</sub> (4)	3,465	1,639	965	535	778	1,115, 612

the loss of coordinated water molecule.<sup>[23,32]</sup> Theoretically calculated weight loss for water molecule was calculated to be 5.01%. So, both the experimental and theoretical values are in close agreement. The peak shifting of C=O group of free chalcones in 1,600–1,700 region to lower frequency in complexes vouch for the coordination of ligand to metal through C=O group,<sup>[23]</sup> which was further confirmed by appearance of M—O peak in region 520–550 cm<sup>-1</sup>.<sup>[33,34]</sup> The presence of sulphate ion was supported by the emergence of two prominent peaks around wavelengths 1,100 and 600. Further, the nonsplitted nature of the vibrational band at 1,110–1,120 cm<sup>-1</sup> in complexes supported the ionic nature of the sulphate group.<sup>[35]</sup> The oxido-vanadium complexes show their characteristic V=O band at 950–980 cm<sup>-1</sup> in the spectrum.<sup>[36]</sup> The appearance and shifting of IR spectral peaks in the complexes are given in Table 1.

**FIGURE 1** Thermogravimetric analysis curve of [VO (L<sup>III</sup>)<sub>2</sub>(H<sub>2</sub>O)<sub>2</sub>]<sub>2</sub>SO<sub>4</sub> (3)

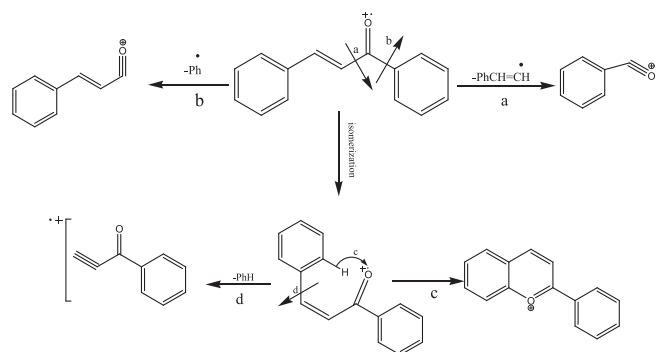
### 3.1.2 | <sup>1</sup>H and <sup>13</sup>C NMR spectral data for ligands

Formation of all the synthesized ligands was further characterized using <sup>1</sup>H NMR (Figures S9–S12) and <sup>13</sup>C NMR (Figures S13–S16) spectral technique. The appearance of peculiar doublet for the newly formed olefinic bond was observed at 7.83 and 7.52 ppm for L<sup>I</sup>, at 8.22 and 7.97 ppm for L<sup>II</sup>, at 7.9 and 7.86 ppm for L<sup>III</sup> and at 7.08 and 7.43 ppm for L<sup>IV</sup>. In <sup>13</sup>C spectrum, distinct peaks appeared corresponding to Olefinic C=C bond and C=O functional at 122.7, 144.7 and 190.5 ppm for Group L<sup>I</sup>; at 123.6, 138.3 and 194.3 ppm for L<sup>II</sup>; 122.3, 141.7 and 189.6 ppm for L<sup>III</sup>; 119.7, 144.7 and 190.5 for L<sup>IV</sup>. In <sup>1</sup>H NMR spectra, appearance of singlet peaks at 10.03 ppm and 3.86 ppm due to hydroxyl proton of L<sup>I</sup> ligand and methoxy protons of L<sup>IV</sup> respectively were the few characteristic peaks along with the other important peaks (as given in above section in synthesis part) which confirmed the synthesis of the ligands L<sup>I-IV</sup>.

### 3.1.3 | Mass spectral data

The mass spectral data of the ligands (Figures S17–S20) and complexes (Figures S21–S24) have further supported the formation of vanadyl chalcone complexes. The recorded mass spectrum of ligands (L<sup>I-IV</sup>) displayed the (M + H<sup>+</sup>) ion peak at m/z 209, 225, 254 and 239, respectively. Further, series of fragmented ion peaks for the ligands were observed according to their general fragmentation pattern<sup>[37]</sup> as given as follows in Scheme 4.

Molecular ion peak for Complex 1 (M + K<sup>+</sup>) was observed at m/z value 654. Series of daughter ions peaks at 543 (for complex-SO<sub>4</sub> + Na), 429 (for VO(L<sup>I</sup>)(C<sub>9</sub>H<sub>7</sub>O<sup>+</sup>)), 274 (for VO(L<sup>I</sup>), 207 (L<sup>I</sup>) and 144 (C<sub>7</sub>H<sub>5</sub>O + K<sup>+</sup>). For Complex 2, the following daughter ion peaks were observed: 480 ([VO (L<sup>II</sup>)<sub>1</sub>(H<sub>2</sub>O)<sub>2</sub>(C<sub>9</sub>H<sub>7</sub>O)]Na<sup>+</sup>, 470 ([VO (L<sup>II</sup>)<sub>1</sub>(H<sub>2</sub>O)<sub>2</sub>(C<sub>7</sub>H<sub>5</sub>O)]K<sup>+</sup>, 430 ([VO (L<sup>II</sup>)<sub>1</sub>(H<sub>2</sub>O)<sub>2</sub>(C<sub>7</sub>H<sub>5</sub>O)]



**SCHEME 4** General pattern of fragmentation of chalcone molecule into daughter ions

$H^+$ , 308 ( $[VO(L^{II})_1(H_2O)_1]$ ), 313  $[VO(L^{II})Na^+]$ , 263 ( $L^{II}K^+$  and 207 ( $L^{II}-OH$ ). For Complex 3, molecular ion  $M^+$  was at 704  $m/z$  value. The fragmented ions at few  $m/z$  values may be inferred as at 679 for  $[VO(L^{III})_2(H_2O)_2]SO_4 + Na$ , 474 for  $[VO(L^{III})_1(C_9H_7O)]Na^+$ , 342 for  $(VOL^{III})Na^+$  and 276 for  $(L^{III}) + Na^+$ . Similarly, for Complex 4,  $M^+$  was at 674. The mass spectrum shows distinctive peaks at 239 (for  $L^{IV} + H^+$ ), 340 [for  $VO(L^{IV})(H_2O)_2]$  and 540 (for  $[VO(L^{IV})(H_2O)_2(C_{10}H_9O_2)]K^+$  daughter ion.

### 3.1.4 | Conductance measurement and gravimetric analysis for complexes $[VO(L^{I-IV})_2(H_2O)_2]SO_4$ (1–4)

Molar conductance measurement gives valuable information about the electrolytic behaviour of the complexes. The position of the sulphate ion group in the complex can further be verified firmly by measuring molar conductance in mM solution of DMSO (Table 2).<sup>[38]</sup> Molar conductance values were in the range of  $50\text{--}90 \Omega^{-1} \text{cm}^{-1} \text{mol}^{-1}$ , which indicates 1:1 electrolytic behaviour.<sup>[39]</sup> This validates the presence of sulphate ion in ionization sphere. Also gravimetrically, all the complexes give white-coloured precipitates of barium sulphate when treated with barium chloride solution as presented in Scheme 5.

### 3.1.5 | EPR data

The X-band EPR spectrum for powdered vanadium (IV) complexes was measured at room temperature. EPR study of powder sample gives valuable information regarding the structure of the complex.<sup>[40]</sup> EPR spectra for all the 4 complexes are given in Figure 2. The spectrum consists of a broad anisotropic curve as a characteristic peak without any hyperfine splitting.<sup>[41]</sup> The  $g_{iso}$  value was calculated from the spectra using the following equation:

$$g = \frac{h \times f}{m_B \times B}, \quad (5)$$

where  $h$  = Planck's constant ( $6.62 \times 10^{-34}$  J. S),  $f$  = frequency (Hz),  $B$  = magnetic field (in Tesla) and  $m_B$ : Bohr magneton =  $9.2740154 \times 10^{-24}$  J/T

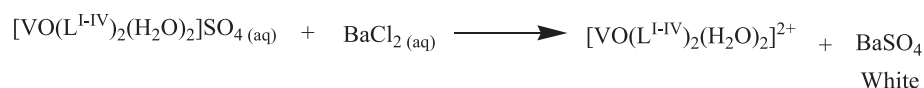
The observed lower  $g_{iso}$  value than  $g$  value for the free electron ( $g_e = 2.0023$ ) supports the fact that the complex is axially symmetrical (Table 3). The lowering in  $g$  values may be associated with a spin-orbit interaction of ground-state and low-lying excited states.<sup>[41]</sup> The study of Garribba and Micera<sup>[42]</sup> showed that geometry of metal with less-than-half-filled electronic configuration always has lower values of  $g_{iso}$  than that of a free electron. Moreover,  $g_{iso}$  value indicated that a complex molecule was displaying a square pyramidal geometry.<sup>[36]</sup>

### 3.1.6 | Geometry of the complexes

The electronic spectrum (Figure S25) of Complex 3 display bands at 308 and 342 nm which were assigned to ligand-metal charge transfer transition in the complex. Absorption of bands at 390 and 559 nm were assigned to spin allowed to  ${}^2B_2 \rightarrow {}^2A_1$  and  ${}^2B_2 \rightarrow {}^2B_1$  transitions, respectively. This pattern of absorption corroborates for the square pyramidal geometry of the complex,<sup>[43]</sup> as described in EPR spectrum data analysis. The TGA thermogram (as illustrated in Figure 1) showed the decomposition steps. Weight loss of 4.9% was observed at  $142^\circ\text{C}$  temperature, which was assigned to the loss of

**TABLE 2** Physical properties of metal chalcone complexes

Sr. No.	Complexes	Melting point	% yield	Molar conductance ( $\Omega^{-1} \text{cm}^2 \text{mol}^{-1}$ )
1.	$[VO(L^I)_2(H_2O)_2]SO_4$ (1)	$>300^\circ\text{C}$	69.33	54.15
2.	$[VO(L^{II})_2(H_2O)_2]SO_4$ (2)		76.30	89.32
3.	$[VO(L^{III})_2(H_2O)_2]SO_4$ (3)		62.59	50.32
4.	$[VO(L^{IV})_2(H_2O)_2]SO_4$ (4)		48.21	53.29



**SCHEME 5** Gravimetric analysis of vanadium chalcone complexes

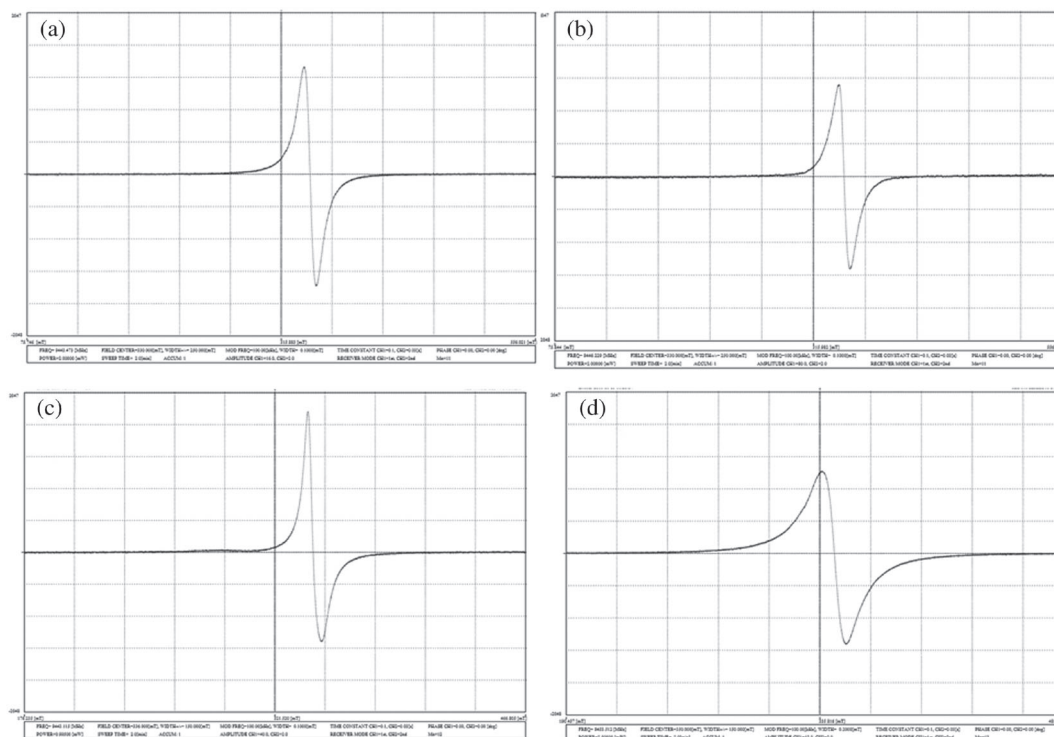


**FIGURE 2** Experimental X-Band electron paramagnetic resonance spectra of complexes: (a) Complex 1, (b) Complex 2, (c) Complex 3 and (d) Complex 4

**TABLE 3**  $g_{\text{iso}}$  values of the complex molecules

Complexes	$g_{\text{iso}}$
$[\text{VO}(\text{L}^{\text{I}})_2(\text{H}_2\text{O})_2]\text{SO}_4$ (1)	1.9978
$[\text{VO}(\text{L}^{\text{II}})_2(\text{H}_2\text{O})_2]\text{SO}_4$ (2)	1.9869
$[\text{VO}(\text{L}^{\text{III}})_2(\text{H}_2\text{O})_2]\text{SO}_4$ (3)	1.9856
$[\text{VO}(\text{L}^{\text{IV}})_2(\text{H}_2\text{O})_2]\text{SO}_4$ (4)	1.9993

coordinated water molecule, 12.85% weight loss (calcd. 13.04%) in range 420°C–480°C for loss of  $\text{NO}_2$  of ligands and 14.2% weight loss (calcd. 13.8%) at 584°C for the  $\text{SO}_4$  group.<sup>[23,32]</sup> The higher char value even at 800°C represents the high thermal stability of the complex. The decomposition steps are shown in Scheme 6.

Further, magnetic nature and magnetic moment of the complex were measured from the hysteresis loop of vibrating sample magnetometer spectrum (Figure 3) at room temperature. The magnetic hysteresis loop of Complex 3 displays a characteristic pattern of dominant paramagnetic component along with little impurity of

ferromagnetic component. The value of magnetic moment measured from the hysteresis curve was found to be 1.56 B.M., which also favourably validates the square pyramidal geometry of V (IV) complex with one unpaired electron.<sup>[44]</sup> From the spectrum, it has been observed that magnetization decreases to zero with the decrease in magnetic field, and loop closes at 1.48 T. On application of magnetic field in reverse direction, negative values of magnetization appear, and loop closes at -1.48 T. This positive slope of loop or curve shows the paramagnetic nature of complex.<sup>[45]</sup> Based on the evaluated data from the characterization techniques, tentative structure of the complexes is given as follows in Scheme 7.

### 3.1.7 | Surface morphology

SEM was employed to monitor the surface morphology of the ligands and their vanadyl complex. The resulting images are shown in Figures 4 and 5 for ligands ( $\text{L}^{\text{I-IV}}$ ) and their vanadyl complexes (1–4), respectively. From

**SCHEME 6** Decomposition steps of Complex 3 according to thermogravimetric analysis thermogram

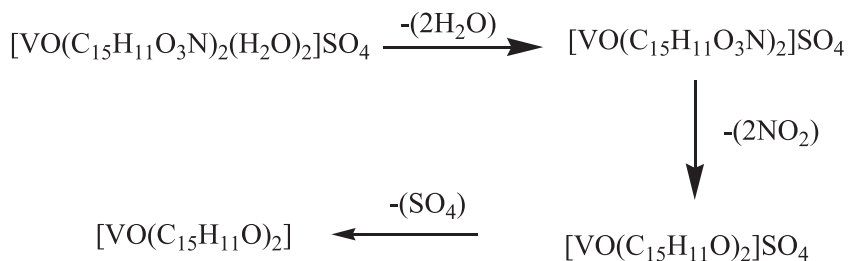
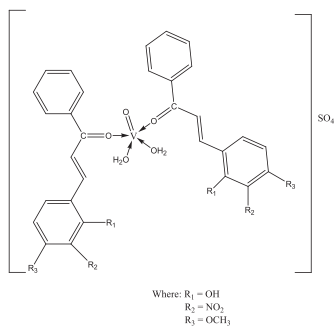
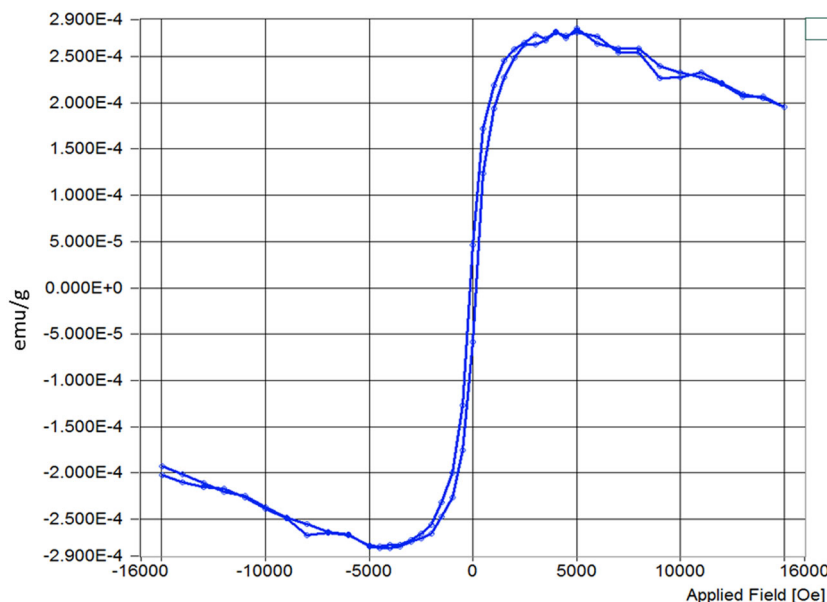


**FIGURE 3** Vibrating sample magnetometer spectrum of Complex 3



**SCHEME 7** Purposed structure of synthesized complexes

the figures, ligands displayed a platelet-like structure.<sup>[46]</sup> These platelet-like structures got agglomerate upon complexation with vanadyl sulphate and is compacted in appearance than that in case of ligands. On comparing the SEM images of ligands and complexes, a significant change in surface morphology has been observed viz compactness of the structure, fewer void spaces and reduction in soft and spongy nature.<sup>[47]</sup> This confirmed the coordination of ligands to the vanadium metal. It was further supported by the energy dispersive X-ray analysis (EDX) data of complexes (Figures S26–S29; Tables S1–

S4), which show the presence of all the functional groups in complexes viz Vanadium, sulphur, oxygen, carbon and nitrogen. However, percentage of elements present cannot be conferred correctly as EDX cannot detect hydrogen atom.<sup>[48]</sup>

## 3.2 | Biophysical evaluation

### 3.2.1 | Antioxidant capacity

Formation of reactive free radicals and oxygen species increases due to the hyperglycemic conditions in diabetes, which depresses the antioxidant system of the body, hence increases cellular damage.<sup>[49]</sup> DPPH radical scavenging assay was used to monitor the antioxidant capacity of vanadyl chalcone complexes. A literature study showed that the efficiency of a particular complex to behave as an antioxidant agent depends upon its ability to donate hydrogen/electron to reduce the DPPH as it is a stable nitrogen-centred free radical.<sup>[50]</sup> Among all the ligands, only L<sup>II</sup> with hydroxy derivative was found to be an effective antioxidant agent with IC<sub>50</sub> 273.26 μg/ml. Among all complexes, [VO (L<sup>II</sup>)<sub>2</sub>(H<sub>2</sub>O)<sub>2</sub>]

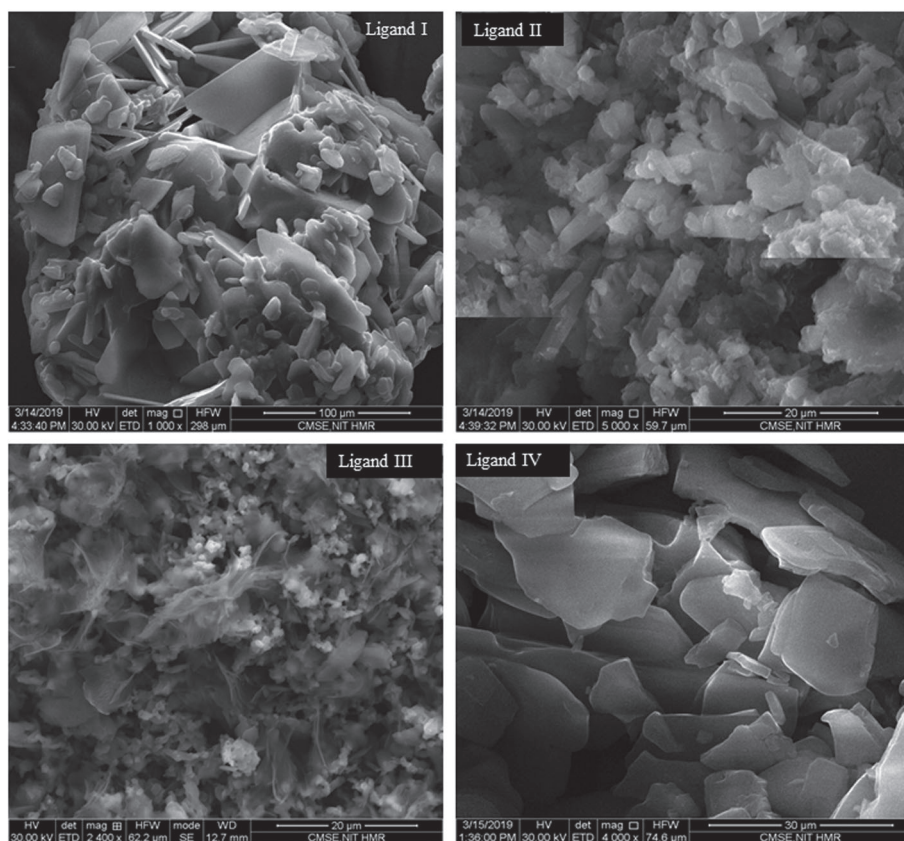


**FIGURE 4** Scanning electron microscope photographs of Ligands I–IV

$\text{SO}_4$  (**2**) and  $[\text{VO}(\text{L}^{\text{IV}})_2(\text{H}_2\text{O})_2]\text{SO}_4$  (**4**) were found to be most potent antioxidant agents in comparison with respective free ligands with  $\text{IC}_{50}$  39.58  $\mu\text{g}/\text{ml}$  and 32.62  $\mu\text{g}/\text{ml}$  values, respectively. This enhancement in the activity of complexes comparative with the ligands can be attributed to the formation of large conjugated system and oxidation of  $\text{V}^{\text{(IV)}}\text{O}^{2+}$  to  $\text{V}^{\text{(V)}}\text{O}^+$  in the system.<sup>[36]</sup> The presence of the hydroxy group in  $\text{L}^{\text{II}}$  may be the active factor for its antioxidant potential. The % inhibition data for ligand and complexes in given Table 4 and shown by the bar graph in Figure 6.

### 3.3 | Biological evaluation

#### 3.3.1 | $\alpha$ -glucosidase inhibition assay

The % inhibition of  $\alpha$ -glucosidase enzyme activity by the synthesized complexes was evaluated by the method described in a report of Ain et al.<sup>[27]</sup> The  $\text{IC}_{50}$  value for all the complexes and standard acarbose was determined from the graph between % inhibition *v/s* concentrations and are given in Table 5. In studies, a continuous decrease was observed in the activity of  $\alpha$ -glucosidase with increasing concentration of the sample in solution. Although % inhibition activity of the complexes was less than that of the standard acarbose which inhibits the

enzyme completely, all the complexes have shown a potent inhibition against  $\alpha$ -glucosidase with  $\text{IC}_{50}$  value ranging in 7.35, 9.15, 3.26 and 8.51  $\mu\text{g}/\text{ml}$  for Complexes **1–4**, respectively. Among all the complexes, Complex **3** with nitro group derivative on  $\text{L}^{\text{III}}$  at *m*-position demonstrated the best inhibitory activity with 3.26  $\mu\text{g}/\text{ml}$   $\text{IC}_{50}$  value. So, introduction of electron withdrawing group enhanced the inhibition activity of the complex. As vanadium complexes possess square pyramidal geometry, they may bind to the  $\alpha$ -glucosidase at active or allosteric site through vacant (sixth) coordination position on vanadium ion. After binding, the establishment of hydrogen and hydrophobic interactions stabilize the inhibitor cooperatively as explained in the study of Misra.<sup>[51]</sup> Further, mode of inhibition was monitored for the complex with the best  $\text{IC}_{50}$ , and it displayed the mixed type inhibition.

#### 3.3.2 | $\alpha$ -amylase inhibition assay

In the present study, ligands ( $\text{L}^{\text{I}}\text{--}\text{L}^{\text{IV}}$ ) and complexes (**1–4**) were screened for the inhibition activity against  $\alpha$ -amylase. The calculated % inhibition and  $\text{IC}_{50}$  value for the ligands and complexes have been presented in Table 6. The inhibition pattern for both ligands and complexes was ascertained to be dose-dependent; viz with the increase of inhibitor concentration, %

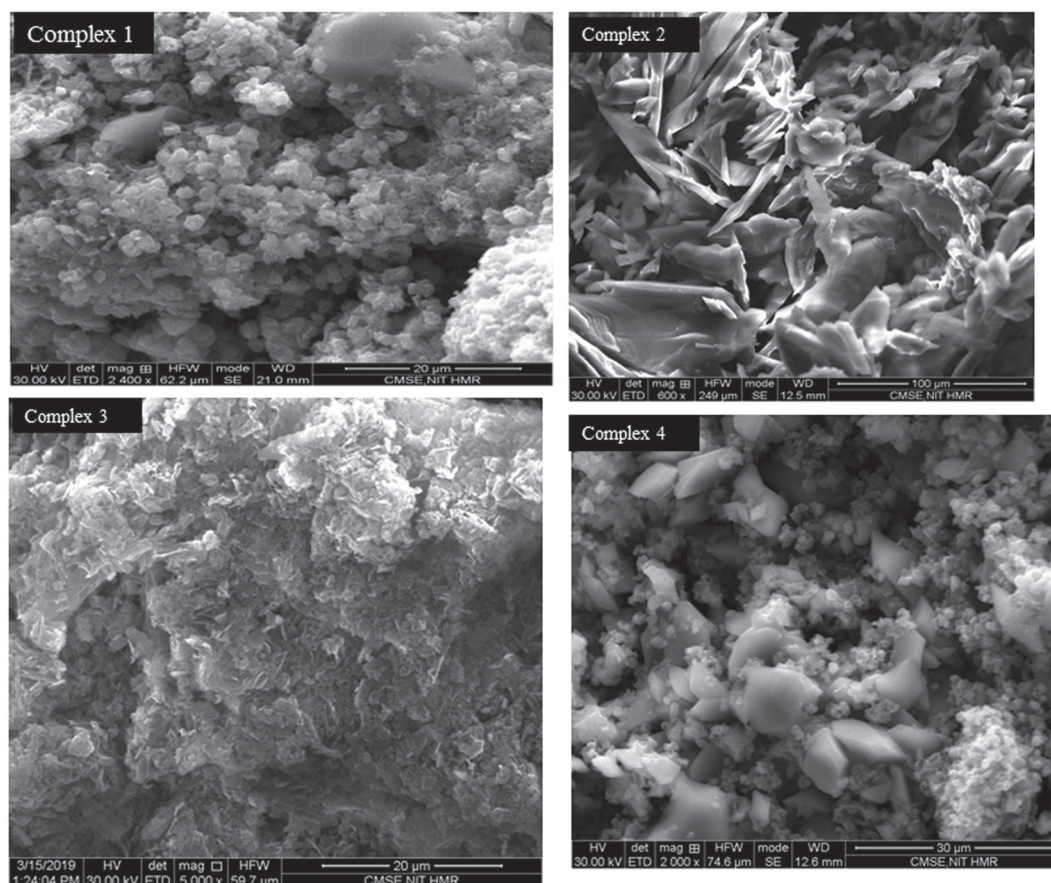


**FIGURE 5** Scanning electron microscope photographs for Complexes 1–4

inhibition increased. From in vitro studies of ligands, no hypoglycemic activity was observed for  $L^I$  and the highest activity for  $L^{IV}$  with 164  $\mu\text{g/ml}$   $\text{IC}_{50}$  value.  $\text{IC}_{50}$  values were calculated from the plot % inhibition *v/s* concentration (in  $\mu\text{M}$ ) to measure the half maximal inhibitory concentration. All the complexes have shown a remarkable and better inhibition activity than ligands against the  $\alpha$ -amylase enzyme. Among the complexes, Complex 2 with  $L^{II}$  was detected to be the most potent

hypoglycemic agent with 302  $\mu\text{g/ml}$   $\text{IC}_{50}$  value, even better than standard acarbose which  $\text{IC}_{50}$  value was found to be 388  $\mu\text{g/ml}$ . The reason behind the better activity of the complexes is may be due to extra structural advantage (increased conjugation and  $\Pi$ -cloud). From the literature studies, it has been established that the active site on the surface of the  $\alpha$ -amylase enzyme is located in V-shaped depression. The predicted square pyramidal geometry of the complexes may bind the

**TABLE 4** Percentage (%) DPPH radical scavenging activity

Ligand/complexes	Concentration ( $\mu\text{M}$ )						$\text{IC}_{50}$ $\mu\text{g/ml}$
	5	20	50	80	100	150	
$L^I$	-	-	-	-	-	-	-
$L^{II}$	42.97	43.96	44.53	44.6	45.5	47.09	273.23
$L^{III}$	-	-	-	-	-	-	-
$L^{IV}$	-	-	-	-	-	-	-
$[\text{VO}(\text{L}^I)_2(\text{H}_2\text{O})_2]\text{SO}_4$ (1)	-	-	-	-	-	-	-
$[\text{VO}(\text{L}^{II})_2(\text{H}_2\text{O})_2]\text{SO}_4$ (2)	44.74	46.81	50.87	54.07	61.07	64.52	39.58
$[\text{VO}(\text{L}^{III})_2(\text{H}_2\text{O})_2]\text{SO}_4$ (3)	-	-	-	-	-	-	-
$[\text{VO}(\text{L}^{IV})_2(\text{H}_2\text{O})_2]\text{SO}_4$ (4)	39.91	45.43	45.92	56.43	59.31	64.14	32.62
Ascorbic acid	86.96	97.18	97.29	97.30	97.82	98.03	

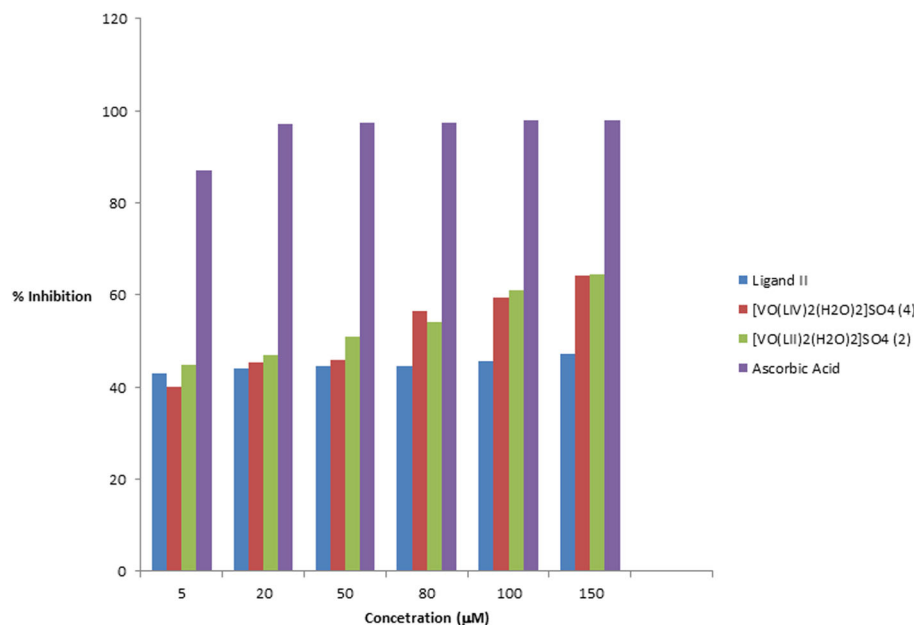


**FIGURE 6** 2,2-diphenyl-1-picryl-hydrazyl-hydrate scavenging activity of ligand (L<sup>I</sup>) and their vanadyl complexes (2 and 4)

active site or at some other site near active sites through hydrogen bonds or other hydrophobic interactions. Thus, block the access to active site of the enzyme or changes the shape or environment around it due to allosteric interaction. So, the enzyme is no longer active for the hydrolysis of the polysaccharide molecule.<sup>[52]</sup>

### 3.3.3 | Enzyme kinetics and mode of inhibition

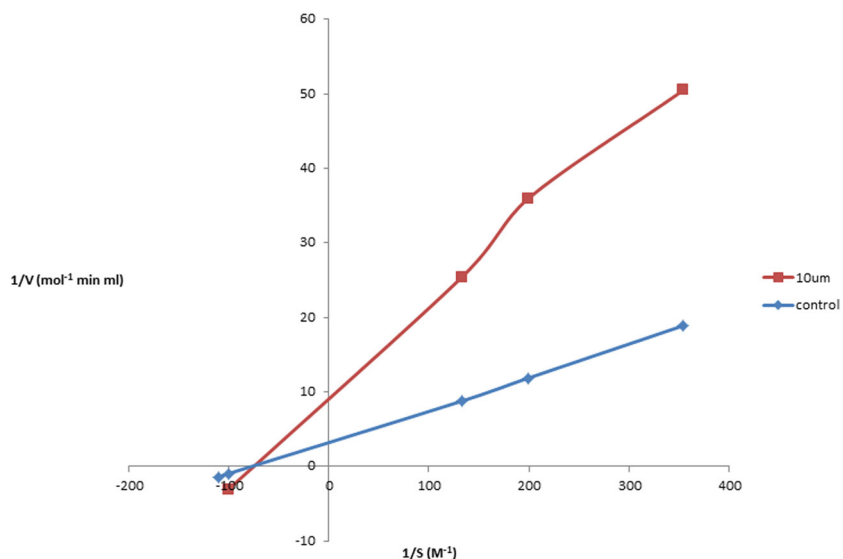
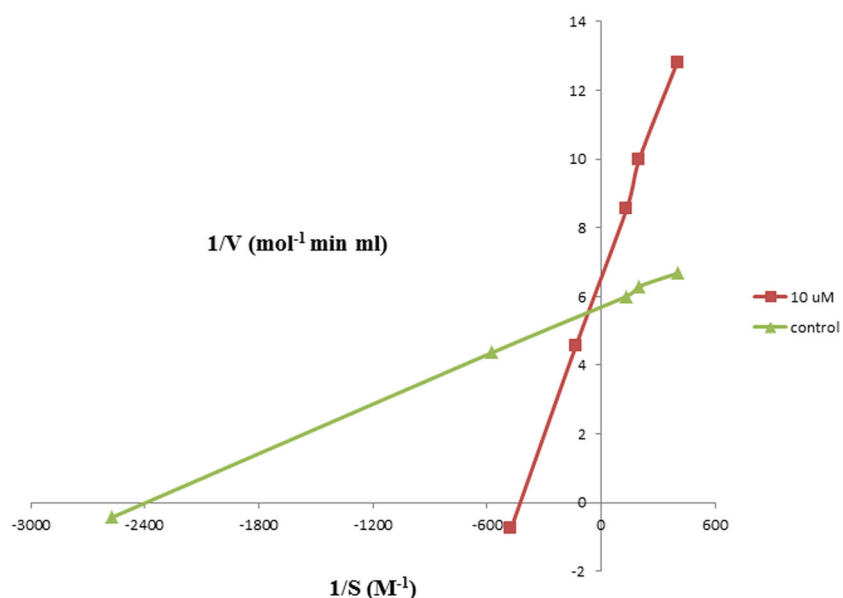
The inhibitors can approach the enzyme in many ways to prevent its activity in the metabolism.<sup>[53]</sup> So, the mechanism of inhibition followed by the complex inhibitors for the enzyme was discerned using the Lineweaver–Burk

**TABLE 5** Percentage (%)  $\alpha$ -glucosidase inhibition activity of [VO (L<sup>I-IV</sup>)<sub>2</sub> (H<sub>2</sub>O)<sub>2</sub>]SO<sub>4</sub> (1–4) complexes

Complexes	Concentration (μM)						IC <sub>50</sub> (μg/ml)
	3	6	10	15	20	50	
% inhibition for [VO (L <sup>I</sup> ) <sub>2</sub> (H <sub>2</sub> O) <sub>2</sub> ]SO <sub>4</sub> (1)	3.58	47.80	71.42	76.79	98.75	99.11	7.35
% inhibition for [VO (L <sup>II</sup> ) <sub>2</sub> (H <sub>2</sub> O) <sub>2</sub> ]SO <sub>4</sub> (2)	8.05	51.91	59.18	60.23	71.81	88.12	9.15
% inhibition for [VO (L <sup>III</sup> ) <sub>2</sub> (H <sub>2</sub> O) <sub>2</sub> ]SO <sub>4</sub> (3)	27.09	72.33	93.67	97.31	98.44	98.71	3.26
% inhibition for [VO (L <sup>IV</sup> ) <sub>2</sub> (H <sub>2</sub> O) <sub>2</sub> ]SO <sub>4</sub> (4)	15.66	18.81	49.82	93.21	94.95	97.58	8.51

**TABLE 6** Percentage (%)  $\alpha$ -amylase inhibition activity of chalcones (L<sup>I-IV</sup>) and [VO (L<sup>I-IV</sup>)<sub>2</sub> (H<sub>2</sub>O)<sub>2</sub>]SO<sub>4</sub> (1–4) complexes

Complexes	Concentration (μM)							IC <sub>50</sub> (μg/ml)
	20	50	80	100	150	300	500	
% inhibition for L <sup>I</sup>	-	-	-	-	-	-	-	-
% inhibition for L <sup>II</sup>	1.58	8.55	12.38	14.66	18.71	24.71	38.07	663
% inhibition for L <sup>III</sup>	9.82	10.41	11.15	12.54	12.71	23.24	38.96	707.59
% inhibition for L <sup>IV</sup>	12	13.8	29.52	41.76	47.79	57.65	76.18	164.06
% inhibition for [VO (L <sup>I</sup> ) <sub>2</sub> (H <sub>2</sub> O) <sub>2</sub> ]SO <sub>4</sub> (1)	6.38	9.52	9.85	16.01	20.91	36.55	92.29	302.52
% inhibition for [VO (L <sup>II</sup> ) <sub>2</sub> (H <sub>2</sub> O) <sub>2</sub> ]SO <sub>4</sub> (2)	0.94	4.29	8.44	11.38	11.97	53.60	62.70	369.42
% inhibition for [VO (L <sup>III</sup> ) <sub>2</sub> (H <sub>2</sub> O) <sub>2</sub> ]SO <sub>4</sub> (3)	4.17	5.37	10.20	10.27	26.11	37.46	53.27	443.18
% inhibition for [VO (L <sup>IV</sup> ) <sub>2</sub> (H <sub>2</sub> O) <sub>2</sub> ]SO <sub>4</sub> (4)	3.90	5.92	7.58	11.64	12.33	34.30	63.14	412.13

**FIGURE 7** Lineweaver–Burk plot for kinetics studies of  $\alpha$ -glucosidase inhibition**FIGURE 8** Lineweaver–Burk plot for kinetic studies of  $\alpha$ -amylase inhibition

plot as given in Figures 7 and 8. The double reciprocal plot between  $1/[S]$  v/s  $1/[V]$  gives a linear relationship, where  $[S]$  is a concentration of substrate and  $[V]$  is the reaction velocity. From the graph, the value of  $V_{\max}$  was calculated from the ordinate intercept as it is equal to  $1/V_{\max}$ , whereas negative abscissa intercept is equal to  $[-1/K_m]$ . The acquired  $K_m$  and  $V_{\max}$  values for both enzymes are presented in Table 7. As observed from the

graph, complexes showed mixed inhibition for both enzymes  $\alpha$ -glucosidase enzyme and  $\alpha$ -amylase. Literature studies revealed that mixed inhibition (i.e., mixture of competitive and uncompetitive inhibition) does not depend whether the substrate is already bound to the enzyme or not. Likewise, the value of  $K_m$  can increase or decrease with the increase in concentration of the inhibitor. From the graphs shown in Figures 5 and 6, it is

**TABLE 7** Kinetic parameters and mode of enzymatic inhibition

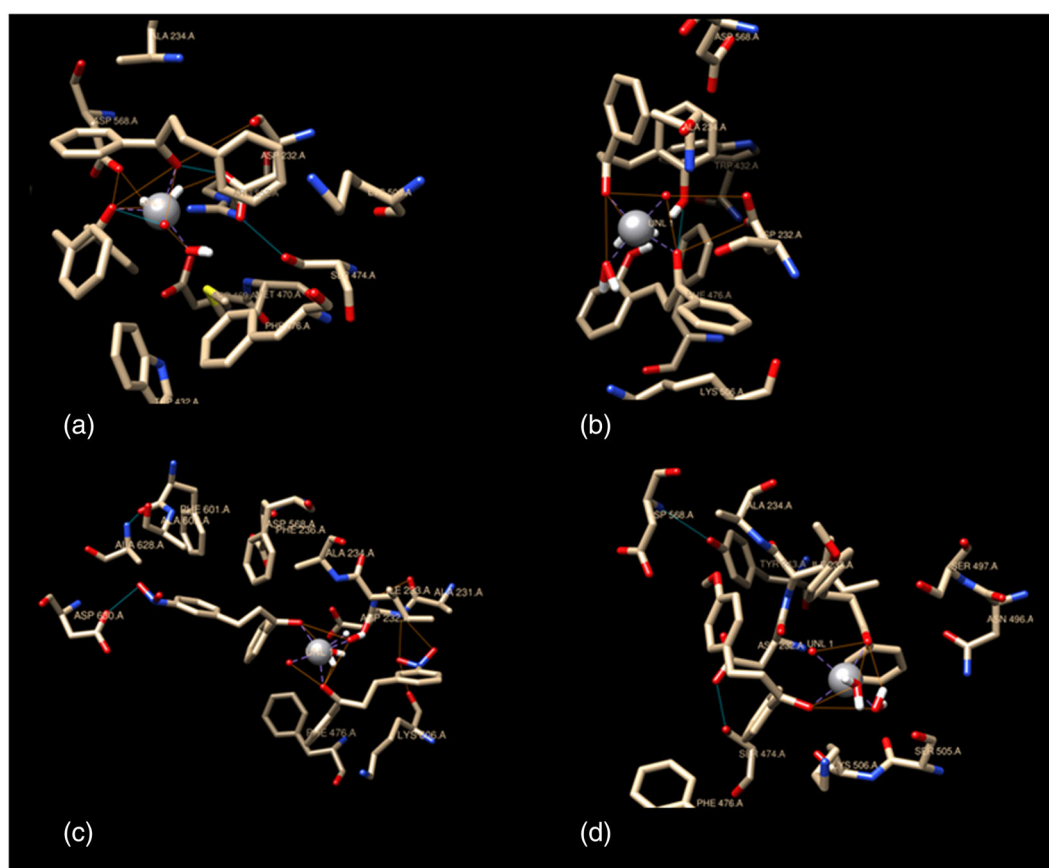
Enzyme	Concentration ( $\mu\text{M}$ )	$V_{\max}$	$K_m$	Type of inhibition
$\alpha$ -amylase	Control 10	0.1743 0.1505	0.0004 0.0023	Mixed
$\alpha$ -glucosidase	Control 10	0.2953 0.1113	0.0128 0.0134	Mixed

**TABLE 8** Mode of interaction and interacting residues for enzymatic inhibition (where UNL = ligand L<sup>I-IV</sup>)

Enzyme	Complex 1	Complex 2	Complex 3	Complex 4
$\alpha$ -amylase	-	H-Asp297, H-Asp340, N-Arg344 with O-UNL	N-Gln35 with O-UNL	-
$\alpha$ -glucosidase	H-Asp232, H-Asp568 with O-UNL	O-Asp232 with O=V	O-Asp630, O-Lys506, and O-Asp232 with O-NO <sub>2</sub>	-

**TABLE 9** In silico kinetic parameters of enzymatic inhibition

Enzyme	Complex	Energy of binding (kcal/mol)	Inhibition constant (Ki)	Electrostatic energy (kcal/mol)	Torsional free energy (kcal/mol)
$\alpha$ -amylase	1	-9.03	242.29 nM	-0.03	+3.84
	2	-11.33	4.99 nM	-0.44	+4.39
	3	-9.91	54.82 nM	-0.04	+4.39
	4	-7.21	5.15 $\mu$ M	-3.11	+4.39
$\alpha$ -glucosidase	1	-8.13	1.09 $\mu$ M	+0.22	+3.84
	2	-8.84	328.72 nM	+0.10	+4.39
	3	-10.02	45.49 nM	+0.06	+4.39
	4	-6.46	18.33 $\mu$ M	-0.46	+4.39

**FIGURE 9** Molecular docking model for complexes with  $\alpha$ -glucosidase: (a) Complex 1, (b) Complex 2, (c) Complex 3 and (d) Complex 4



From in vitro studies, all the complexes found to possess promising activity against the  $\alpha$ -amylase and  $\alpha$ -glucosidase enzyme with  $IC_{50}$  in range 3–9  $\mu\text{g/ml}$  and greater than 100  $\mu\text{g/ml}$  against  $\alpha$ -glucosidase and  $\alpha$ -amylase enzyme, respectively. These results were also supported by the docking studies, and the investigation revealed that the complex molecules interact with the target enzyme through noncovalent H-bonding, van der Waals' and hydrophobic interaction. In addition, DPPH assay was performed to investigate the antioxidant potential of the complexes. From the results, two complexes (Complexes **2** and **4**) have shown good antioxidant potential. So, the vanadyl chalcone complexes as expected have promising antidiabetic and antioxidant agents.

### ACKNOWLEDGEMENTS

The authors express their gratitude towards Department of Material Sciences, NIT Hamirpur, for providing various characterization technique facilities.

### AUTHOR CONTRIBUTIONS

**Mandeep Kaur:** Conceptualization; data curation; formal analysis; investigation; methodology; validation; visualization. **Raj Kaushal:** Conceptualization; data curation; formal analysis; investigation; methodology; resources; software; supervision; validation; visualization.

### DATA AVAILABILITY STATEMENT

The data that support the findings of this study are available in the Supporting Information of this article.

### ORCID

Mandeep Kaur  <https://orcid.org/0000-0003-4672-4787>

Raj Kaushal  <https://orcid.org/0000-0003-0198-581X>

### REFERENCES

- [1] Q. Guo, L. Li, J. Dong, H. Liu, T. Xu, J. Li, *Spectrochim. Acta* **2013**, *106*, 155.
- [2] A. N. Antipov, in *Encyclopedia of metalloproteins*, (Eds: R. H. Kretsinger, V. N. Oversky, E. A. Permyakov), Springer, New York **2013**.
- [3] Y. Tanabe, Y. Nishibayashi, *Coord. Chem. Rev.* **2019**, *381*, 135.
- [4] R. Wever, M. A. Van der Horst, *Dalton Trans.* **2013**, *42*, 11778.
- [5] A. Evangelou, *Crit. Rev. Oncol. Hematol.* **2002**, *42*, 249.
- [6] A. Goc, *Cent. Eur. J. Biol.* **2006**, *1*, 314.
- [7] S. Mondal, M. Mukherjee, K. Dhara, S. Ghosh, J. Ratha, P. Banerjee, A. K. Mukherjee, *Cryst. Growth Des.* **2007**, *7*, 1716.
- [8] K. Pandeya, I. Tripathi, M. K. Mishra, N. Jaiswal, *J. Biol. Sci. Med.* **2016**, *2*, 38.
- [9] G. R. Willsky, L. H. Chia, M. Godzala, P. J. Kostyniaka, J. J. Smeee, A. M. Trujilloe, J. A. Alfanoa, W. Dingc, Z. Hud, D. C. Crans, *Coord. Chem. Rev.* **2011**, *255*, 2258.
- [10] S. Treviño, A. Diaz, *J. Inorg. Biochem.* **2020**, *208*, 111094.
- [11] R. Watson, V. Preedy, S. Zibadi, *Polyphenols in human health and disease*, 1st ed., Academic Press **2013**.
- [12] K. Bharatham, N. Bharatham, K. H. Park, K. W. Lee, *J. Mol. Graphics Modell.* **2008**, *26*, 1202.
- [13] S. Burmaoglu, E. A. Kazancioglu, R. Kaya, M. Kazancioglu, M. Karaman, O. Algul, I. Gulcin, *J. Mol. Struct.* **2020**, *1208*, 127868.
- [14] S. Rocha, D. Ribeiro, E. Fernandes, M. Freitas, *Curr. Med. Chem.* **2018**, *25*, 2257.
- [15] D. Avci, S. Altürk, F. Sönmez, Ö. Tamer, A. Başoğlu, Y. Atalay, B. Z. Kurt, N. Dege, *Mol. Diversity* **2020**.
- [16] A. A. Milibari, E. Y. Matuure, E. M. Gadah, *Health Sci. J.* **2020**, *14*, 701.
- [17] S. R. S. Njonou, J. Boombhi, M. C. E. Etoga, A. T. Timnou, A. M. Jingi, K. N. Efon, E. A. M. Eloumba, M. J. N. Essomba, O. K. Kebiwo, A. N. T. Meke, S. T. Ndjanya, M. D. Yefou, E. Sobngwi, *J. Diabetes Res.* **2020**.
- [18] A. K. Singh, R. Gupta, A. Ghosh, A. Misra, *Diabetes Metab. Syndr.* **2020**, *14*, 303.
- [19] M. Mirzaei, M. Rahmaninan, M. Mirzaei, A. Nadjarzadeh, A. A. D. Tafti, *BMC Public Health* **2020**, *20*, 166.
- [20] D. K. Mahapatra, V. Asati, S. K. Bharti, *Eur. J. Med. Chem.* **2015**, *92*, 839.
- [21] H. Ali, P. J. Houghton, A. Soumyanath, *J. Ethnopharmacol.* **2006**, *107*, 449.
- [22] R. Lhoret, J. L. Chiasson, *International textbook of diabetes mellitus*, 3rd ed., John Wiley & Sons Ltd., UK **2004**.
- [23] F. M. Atlam, M. N. El-Nahass, E. A. Bakr, T. A. Fayed, *Appl. Organomet. Chem.* **2018**, *32*, 3951.
- [24] O. Petrov, Y. Ivanova, M. Gerova, *Cat. Com.* **2018**, *9*, 315.
- [25] P. B. Piste, *Int. J. Curr. Sci.* **2014**, *13*, 62.
- [26] H. Yapatia, S. R. Devinenib, S. Chirumamillaa, S. Kalluru, *J. Chem. Sci.* **2016**, *128*, 43.
- [27] Q. Ain, A. Uzma, A. J. Rifat, S. Muhammad, M. T. Mohammad, *Arab. J. Chem.* **2017**, *10*, 488.
- [28] S. Zhang, S. M. Kim, *Appl. Organomet. Chem.* **2019**, *33*, 5102.23.
- [29] D. Kalita, D. G. Holm, D. V. LaBarbera, J. M. Petrash, S. S. Jayanty, *PLoS ONE* **2018**, *13*, 1.
- [30] M. A. Parisa, B. Rahman, H. M. Hassan, A. Pavlo, P. Mayer, *J. Mol. Struct.* **2017**, *1131*, 258.
- [31] J. Fujita, K. Nakamoto, M. Obayashi, *J. Am. Chem. Soc.* **1956**, *78*, 3963.
- [32] V. Uivarosi, S. F. Barbuceanu, V. Aldea, C. C. Arama, M. Badea, R. Olar, D. Marinescu, *Molecules* **2010**, *15*, 1578.
- [33] A. A. S. Al-Hamdani, A. M. Balkhi, A. Falah, S. A. Shaker, *J. Saudi Chem. Soc.* **2016**, *20*, 487.
- [34] E. R. Agharia, *Chem. Sci. Trans.* **2015**, *4*, 463.
- [35] S. Singh, D. P. Rao, A. K. Yadava, H. S. Yadav, *Org. Chem. Curr. Res.* **2011**, *3*, 106.
- [36] K. Savithri, H. D. Revanasiddappa, *Bioinorg. Chem. Appl.* **2018**, *2*, 1.
- [37] A. R. Raza, A. Sultan, N. Ullah, M. R. Saeed, A. Janjua, K. M. Khan, *Mod. Chem. Appl.* **2016**, *4*, 1.
- [38] M. S. Refat, I. M. El-Deen, M. A. Zein, A. M. A. Adam, M. I. Kobeasy, *Int. J. Electrochem. Sci.* **2013**, *8*, 9894.
- [39] I. Ali, W. A. Wani, K. Saleem, *Synth. React. Inorg. M.* **2013**, *43*, 1162.
- [40] T. R. Bryar, D. R. Eaton, *Can. J. Chem.* **1992**, *70*, 1917.

- [41] B. I. Ceylan, E. Tuzun, Y. Kurt, M. Acikgoz, S. Kahraman, G. Atun, B. Ulkuseven, *J. Sulfur Chem.* **2015**, 36, 434.
- [42] E. Garribba, G. Micera, *J. Chem. Educ.* **2006**, 83, 1229.
- [43] C. R. Cornman, K. M. Geiser-Bush, S. P. Rowley, P. D. Boyle, *Inorg. Chem.* **1997**, 36, 6401.
- [44] M. Nasrollahzadeh, M. Atarod, M. Sajjadi, S. M. Sajadi, Z. Issaabadi, *Intro. Green Techno.* **2019**, 28, 199.
- [45] G. Borah, J. Baruah, D. Kardong, *Indian J. Chem.* **2014**, 53, 1520.
- [46] R. S. Joseyphus, M. S. Nair, *Arab. J. Chem.* **2010**, 3, 195.
- [47] A. R. Patil, K. J. Donde, S. S. Rau, V. R. Patil, R. S. Lokhande, *JCHPS* **2012**, 4, 1413.
- [48] N. Stojilovic, *J. Chem. Educ.* **2012**, 89, 1331.
- [49] S. Sabiu, F. H. O'Neill, A. O. T. Ashafa, *J. Ethnopharmacol.* **2016**, 183, 1.
- [50] H. Dong, X. Yang, J. He, S. Cai, K. Xiao, L. Zhu, *RSC Adv.* **2017**, 7, 53385.
- [51] S. Misra, K. B. Pandeya, A. K. Tiwari, A. Z. Ali, T. Saradamani, S. B. Agawane, K. Madhusudana, *Int. J. Nutr. Metab.* **2012**, 4, 11.
- [52] J. C. Westermann, D. J. Craik, *Comprehensive Natural Products II*, 1st ed., Elsevier Science, Amsterdam **2010**.
- [53] K. Balan, P. Ratha, G. Prakash, P. Viswanathamurthi, S. Adisakwattana, H. Palvannan, *Arab. J. Chem.* **2017**, 10, 732.

### SUPPORTING INFORMATION

Additional supporting information may be found online in the Supporting Information section at the end of this article.

**How to cite this article:** Kaur M, Kaushal R. Synthesis, characterization and  $\alpha$ -amylase and  $\alpha$ -glucosidase inhibition studies of novel vanadyl chalcone complexes. *Appl Organomet Chem.* 2020; e6042. <https://doi.org/10.1002/aoc.6042>